Journal of Molecular Modeling (2026) 32:121
https://doi.org/10.1007/s00894-026-06707-6

RESEARCH

A comprehensive first-principles analysis of the dynamical, structural, mechanical, electronic and thermodynamic properties of full-Heusler alloys X_2MgSi (X = Ru, Rh, Pd)

Gökçen Dikici Yıldız[1] · Yasin Göktürk Yıldız[2] · Murat Çanlı[3] · Nihat Arıkan[4]

Received: 8 December 2025 / Accepted: 27 March 2026 / Published online: 6 April 2026

Abstract

Context Full-Heusler alloys X_2MgSi (X = Ru, Rh, Pd) crystallizing in the cubic $L2_1$ structure have been investigated via first-principles density functional theory to fill the knowledge gap regarding their mechanical stability, electronic structure, lattice dynamics, and thermodynamic behavior. The optimized lattice constants are 5.986 Å (Ru_2MgSi), 5.997 Å (Rh_2MgSi), and 6.167 Å (Pd_2MgSi), in good agreement with available theoretical data. The negative formation enthalpies (-0.432, -0.682, and -0.527 eV/atom, respectively) confirm thermodynamic stability and experimental synthesizability. The electronic band structures and density of states reveal metallic characteristics for all three compounds, with the highest density of states at the Fermi level (3.389 states/eV·cell) obtained for Ru_2MgSi. The calculated elastic constants satisfy the Born–Huang stability criteria, and the derived polycrystalline moduli decrease from 198.4 GPa (Ru_2MgSi) to 135.4 GPa (Pd_2MgSi). Pugh's ratio (B/G > 1.75), positive Cauchy pressure, and Poisson's ratio (0.31–0.42) consistently indicate ductile behavior, with Pd_2MgSi exhibiting the highest ductility. The phonon dispersion curves display no imaginary frequencies, confirming the dynamic stability; distinct phonon bandgaps arise from the large mass differences between the constituent atoms. The thermodynamic properties obtained via the quasiharmonic Debye model yield Debye temperatures of 457.6 K (Ru_2MgSi), 392.7 K (Rh_2MgSi), and 223.2 K (Pd_2MgSi), correlating with the trend in elastic stiffness.

Methods This research employs ab initio density functional theory methods implemented within the Quantum ESPRESSO package to explore the structural, elastic, electronic, thermodynamic, and phonon characteristics of X_2MgSi (X = Ru, Rh, and Pd) full-Heusler compounds with the generalized gradient approximation (GGA-PBE) and projector augmented wave (PAW) pseudopotentials. Elastic constants were obtained from the energy-strain method, phonon dispersions from density functional perturbation theory (DFPT), and thermodynamic properties from the quasi-harmonic Debye model. A variety of material properties were accurately identified via first-principles computational methods. Through the quasiharmonic approximation, the thermodynamic behavior of the compounds was examined, revealing for the first time the temperature-dependent variations in internal energy, free energy, specific heat, and entropy.

Keywords First principles · Density function theory · Full-Heusler alloys

✉ Murat Çanlı
murat.canli@ahievran.edu.tr

[1] Department of Physics, Faculty of Arts and Sciences, Kırıkkale University, Kırıkkale 71450, Turkey

[2] Department of Electronics and Automation, Kırıkkale University, Kırıkkale 71480, Turkey

[3] Department of Chemistry and Chemical Processing Technologies, Kırsehir Ahi Evran University, Kırşehir 40500, Turkey

[4] Department of Physics, Faculty of Engineering and Natural Sciences, Osmaniye Korkut Ata University, Osmaniye 80010, Turkey

Introduction

Intermetallic compounds known as Heusler alloys, originally observed by Friedrich Heusler in the early twentieth century, have attracted much attention because of their wide-ranging functionalities. These materials, particularly those adopting the full-Heusler structure denoted X_2YZ, exhibit a diverse array of properties such as spin polarization, magnetism, thermoelectricity, and even superconductivity [1–3]. Structurally, full-Heusler compounds crystallize in a cubic $L2_1$ configuration (space group $Fm\bar{3}m$), where X and Y typically represent transition metals, and Z belongs to the main-group

of elements [4]. The growing interest in Heusler alloys stems from their flexible electronic structures and ability to fine-tune their physical behavior through compositional variation in metals.

Among all metals, magnesium-based Heusler compounds stand out because of the inherent advantages of magnesium as a lightweight, earth-abundant, and industrially significant metal [5]. Its widespread utilization in the automotive, aerospace, and metallurgical sectors is closely linked to its low density, excellent machinability, and favorable mechanical performance [5, 6]. Beyond traditional structural uses, Mg-based compounds have also been investigated in emerging areas such as thermoelectric devices, next-generation Mg-ion batteries, and other functional electronic applications [7, 8]. The combination of lightweight Mg with transition metals such as Ru, Rh, and Pd offers a unique opportunity to tailor mechanical and electronic properties for applications ranging from lightweight structural components to next-generation thermoelectric generators and electrical interconnects.

The increasing reliance on theoretical approaches and advanced computational tools for predicting and tailoring novel Heusler alloys—thereby avoiding the high costs associated with experimental synthesis—has motivated us to conduct a comprehensive investigation of these systems. In this study, density functional theory (DFT) was employed to explore the structural, elastic, electronic, vibrational, and selected thermodynamic characteristics of X_2MgSi (X = Ru, Rh, Pd) full-Heusler alloys. To our knowledge, there are very limited systematic or detailed reports on these alloys in the available literature [9–11].

A review of the literature reveals that no experimental studies have been previously reported on the physical properties of X_2MgSi (X = Ru, Rh, and Pd) alloys, and a narrow range of theoretical studies exist. This study is designed to address this gap in the available literature by contributing a comprehensive analysis of their physical properties. The article is structured as follows: Sect. 2 presents the methodology of the computational approach, Sect. 3 discusses the findings obtained for structural, electronic, elastic, thermodynamic, and phonon properties, and Sect. 4 summarizes the main results.

Computational method

The first principles calculations were completed within the paradigm of density functional theory (DFT) [12]. The structural, electronic, elastic, thermodynamic and phonon characteristics of the investigated alloys were elucidated by leveraging the pseudopotential plane-wave approach [13], as operationalized in the Quantum ESPRESSO simulation suite [14]. The exchange–correlation interactions were delineated by the Perdew–Burke–Ernzerhof (PBE) form of the generalized gradient approximation (GGA) [15]. The interaction of the nuclei-valence electrons was intended using the projector augmented wave (PAW) based pseudopotential. A kinetic energy cutoff of 60 Ry was set for the plane-wave basis, whereas a cutoff of 600 Ry was employed for the electronic charge density. To ensure reliable and accurate results, convergence criteria were defined with a mixing parameter of 0.7 and a threshold of 10^{-9} Ry. The Kohn–Sham equations [16] were solved self-consistently using a Monkhorst–Pack k-point mesh [17] of $10 \times 10 \times 10$ within the Brillouin zone, achieving an energy convergence of 1 mRy per atom. This k-point grid was employed for all self-consistent field (SCF) calculations, including structural relaxations and total energy evaluations. For non-self-consistent (NSCF) calculations, specifically the density of states (DOS) and electronic band structures, a denser $12 \times 12 \times 12$ k-point mesh was utilized to ensure accurate spectral properties. Convergence tests confirmed that further increases in k-point density did not alter the total energy by more than 0.1 mRy/atom or the electronic structure features of interest. Following these calculations, the lattice vibrational properties were acquired with self-consistent density functional perturbation theory (DFPT) [18, 19]. Dynamical matrices were simulated over a $4 \times 4 \times 4$ q-point grid, and inverse Fourier transformation was employed to extract phonon spectra and the vibrational density of states. Elastic constants were derived via the energy-strain technique implemented in the thermo_pw module [20, 21]. Furthermore, thermodynamic quantities such as heat capacity, entropy, and vibrational energy were estimated using the Debye model, as outlined in Ref. [22], through calculations also performed with the thermo_pw utility.

Structural properties

The crystal structures of X_2MgSi (X = Ru, Rh, and Pd) alloys, that all crystallize in the Fm3m space group with four atoms per unit cell, are shown in Fig. 1, where the geometry of X_2MgSi compounds has been optimized. There are 16 atoms in the X_2MgSi alloys that crystallize in the Fm3m (225) space group in the cubic crystal system, of which the X atoms are 8c (0.25 0.25 0.25), Mg atoms 4a (0 0 0), Si atoms 4b (0.5 0.5 0.5) Wyckoff they are in atomic positions (Fig. 1). The Mg atom is bonded to eight equivalent X atoms in a body-centered cubic geometry. X atom is bonded to four equivalents of Mg and four equivalents of Si atoms in a body-centered cubic geometry. The Si atom is connected to eight equivalent X atoms in a distorted body-centered cubic geometry [23]. Geometric optimization enables the determination of a material's ground-state structural parameters. For X_2MgSi (X = Rh, Ru, and Pd), the stable structural configuration and corresponding lattice constants were confirmed using the GGA

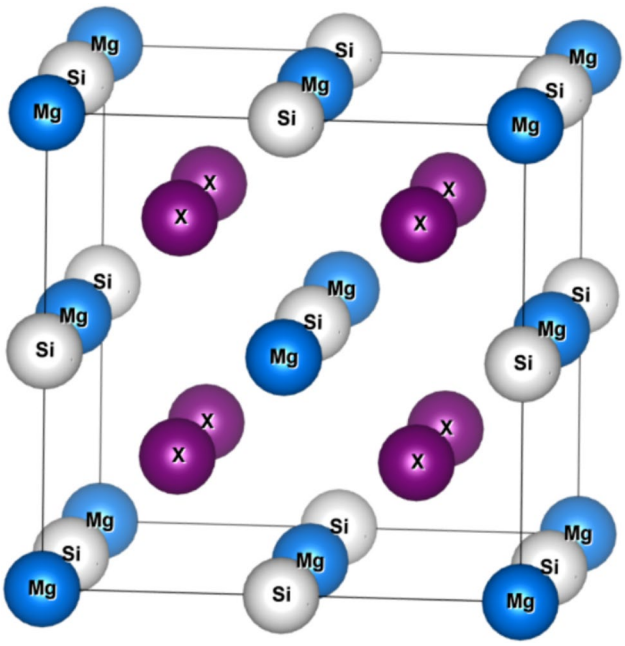

Fig. 1 The unit cell of full Heusler alloys X_2MgSi (X = Ru, Rh, Pd)

approach. Additionally, the obtained structural parameters are stated in Table 1. As shown in the table, the equilibrium lattice constants are consistent with the reported literature values [9–11]. The systematic increase in the lattice constant from Ru_2MgSi (5.986 Å) to Pd_2MgSi (6.167 Å) correlates directly with the increasing atomic radii of the X-site elements (Ru: 134 pm, Rh: 134 pm, Pd: 137 pm). In contrast, the bulk modulus (B) decreases from 198.399 GPa (Ru_2MgSi) to 135.361 GPa (Pd_2MgSi), reflecting the inverse relationship between B and the equilibrium volume. This trend originates from the progressive filling of d-orbitals across the 4 d and 5 d series, which alters the charge distribution and reduces the cohesive energy density. To evaluate the thermodynamic stability and likelihood of synthesizing these alloys, the formation enthalpy of X_2MgSi (X = Ru, Rh, and Pd) is determined with the following equation [22]:

$$\Delta H_f = E_{T_{(MgSiX_2)}} - (E_{(Mg)} + E_{(Si)} + 2E_{(X)}) \quad (1)$$

In this equation, $E_{T(X2MgSi)}$ represents the total energy of the alloys in the $L2_1$ structure, while $E_{(Mg)}$, $E_{(Si)}$, and $E_{(X)}$ denote the computed total energies of the constituents in their most durable reference states. The calculation of the formation enthalpies (Table 1) revealed that negative values of the enthalpies suggest both thermodynamic stability and the potential for experimental synthesis [24, 25]. These results, derived from Eq. (1), confirm the feasibility and stability of these alloys. Furthermore, the data obtained align well with previously reported values. Rh_2MgSi has the most negative enthalpy of formation (–0.682 eV/atom) among all the compounds, indicating the strongest thermodynamic driving force for synthesis. This is attributed to the optimum hybridization between the Rh 2 d and Si 3p states, which maximizes the covalent bond contribution. On the other hand, Ru_2MgSi has weak bonding characteristics (–0.432 eV/atom).

The negative formation enthalpies (Table 1) provide the necessary conditions for thermodynamic stability, indicating that the compounds are energetically favorable with respect to their elemental constituents. However, a complete assessment of thermodynamic stability would require a convex hull analysis that considers all competing binary and ternary phases in the X–Mg–Si system (X = Ru, Rh, Pd). Such an analysis is beyond the scope of the present study, but the negative formation energies reported here, together with the good agreement with the Open Quantum Materials Database (OQMD) values [10], support the synthesizability of these alloys. Future experimental and computational work may further confirm their ground-state stability via full convex hull construction.

Electronic band properties

The electronic band structures and the corresponding total and partial density of states (DOS) are depicted in Fig. 2. The Fermi level has been aligned to zero in the band structure representations. As observed from the band diagrams in Fig. 3, the valence and conduction bands touch the Fermi

Table 1 The evaluated lattice parameters (a, Å), formation enthalpies (ΔH_f, eV/atom), and elastic moduli (C_{11}, C_{12}, C_{44}, in GPa) for the X_2MgSi (X = Ru, Rh, Pd) alloys

Material	*References*	a_0 (Å)	ΔH_f	C_{11}	C_{12}	C_{44}
Ru_2MgSi	This work	5.986	−0.432	318.463	138.367	80.108
	[10]	6.003	−0.352			
Rh_2MgSi	This work	5.997	−0.682	250.165	150.867	72.520
	[11]	6.018	−0.770			
	[10]	6.003	−0.775			
	[9]		−0.248			
Pd_2MgSi	This work	6.167	−0.527	148.068	129.008	33.121
	[10]	6.140	−0.626			

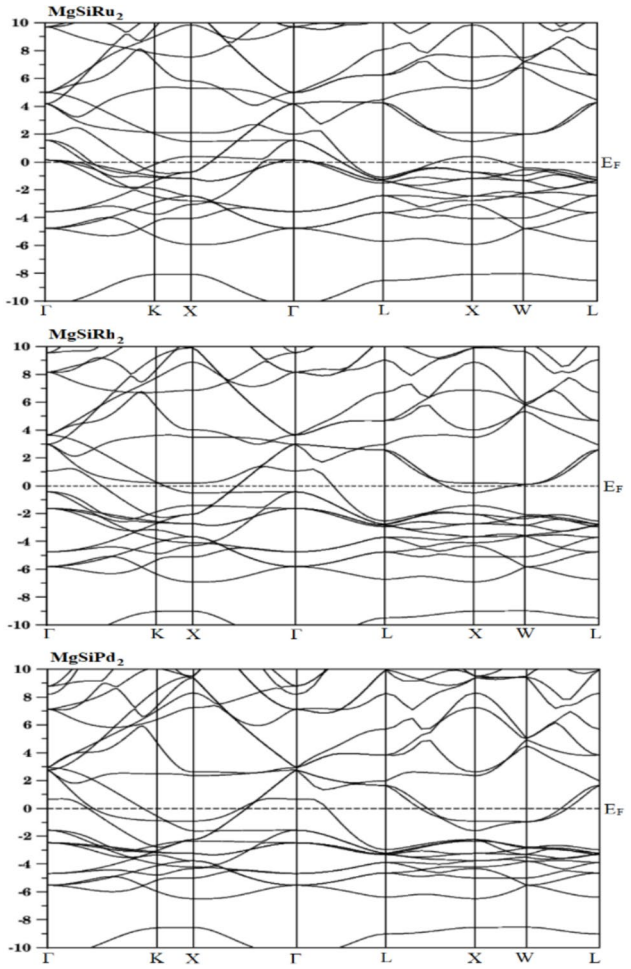

Fig. 2 The computed electronic band profiles of full Heusler alloys X_2MgSi (X = Ru, Rh, Pd)

level for all the examined alloys. This continuous band overlap at the Fermi energy indicates that all the studied compounds exhibit metallic behavior. Therefore, on the basis of the analysis of the electronic structure, it can be concluded that all the alloys under investigation are metallic. The three compounds exhibited similar band structure patterns.

The density of states at the Fermi level, $N(E_F)$, which reflects the metallic nature of the compounds, was 3.389, 0.850, and 1.648 states/eV·cell for Ru_2MgSi, Rh_2MgSi, and Pd_2MgdSi, respectively. The exceptionally high $N(E_F)$ in Ru_2MgSi arises from the sharp d-band peak crossing the Fermi level, a characteristic feature of early transition metal compounds. This suggests that compared with its Rh and Pd counterparts, Ru_2MgSi has a higher electronic conductivity. The metallic nature of Ru_2MgSi originates mainly from the Ru 4 d states, while in Rh_2MgSi it is predominantly governed by the Rh 4 d orbitals. For Pd_2MgSi, the metallic character is driven primarily by contributions from both the Pd 5 d and Si 2p electronic states. The total and partial density of states presented in Fig. 3 reveal that the energy bands extending from the Fermi level down to approximately –6 eV predominantly arise from the 4 d orbitals of Ru (Rh, and Pd) atoms, depending on the specific alloy. Additionally, the electronic states located above the Fermi energy display a widely spread band character and are composed of many contributing states, facilitating metallic conduction. The metallic behavior of these alloys is fundamentally governed by the partially filled d-states of the X-site transition metals. The progressive filling of the d-band from Ru ($4d^7$) to Rh ($4d^8$) to Pd ($4d^{10}$) shifts the Fermi level relative to the d-band center, modulating the charge carrier concentration and electronic transport properties. For Rh_2MgSi, the d-band is narrower and shifted slightly downward, reducing $N(E_F)$. In Pd_2MgSi, the Pd 5 d orbitals are more diffuse and energetically elevated, leading to enhanced mixing with Si 2p states and a more complex band structure near E_F.

Elastic properties

In crystalline structures, differences in structural forces, the nature of bonding between atoms, and the spacing between atoms lead to varying responses of materials to external forces. These variations in the atomic configuration and bonding result in significant differences in elastic behavior. For X_2MgSi (X = Ru, Rh, and Pd) alloys, which crystallize in a cubic system, elastic behavior is typically governed by three independent elastic constants: C_{11}, C_{12}, and C_{44}. The repsponse of a crystal to uniaxial compression is depicted by two elastic constants, C_{11} and C_{12}, whereas its behavior under shear stress is described by the C_{44} elastic constant. Additionally, these elastic constants provide valuable insight into the stability of materials, and the melting temperature of cubic alloys can be estimated on the basis of the C_{11} elastic constant [26].To assess the mechanical stability of X_2MgSi (X = Ru, Rh, and Pd), the Born-Huang stability criterion [27, 28] are employed, which is expressed as follows for a cubic crystal structure: $C_{11} - C_{12} > 0$; $C_{11} + 2C_{12} > 0$; $C_{44} > 0$.

Satisfying with these conditions ensures that the material is mechanically stable against various types of elastic deformation. In this study, we calculated the elastic constants (C_{11}, C_{12}, and C_{44}) for the $MgSiRu_2$, $MgSiRh_2$, and $MgSiPd_2$ alloys in the $L2_1$ phase and present our estimated values in Table 2. According to the mechanical stability criteria, the alloys examined using the GGA approach exhibited mechanical stability as the elastic constants calculated for all the alloys satisfied the above-mentioned conditions. We also calculated various mechanical properties such as the bulk modulus (B), Voigt shear modulus (G_V), Reuss shear modulus (G_R), Voigt-Reuss-Hill mean shear modulus (G), Young's modulus (E), Poisson's ratio (σ), elastic anisotropy factor (A) and Cauchy pressure (CP) as presented in Table 2;

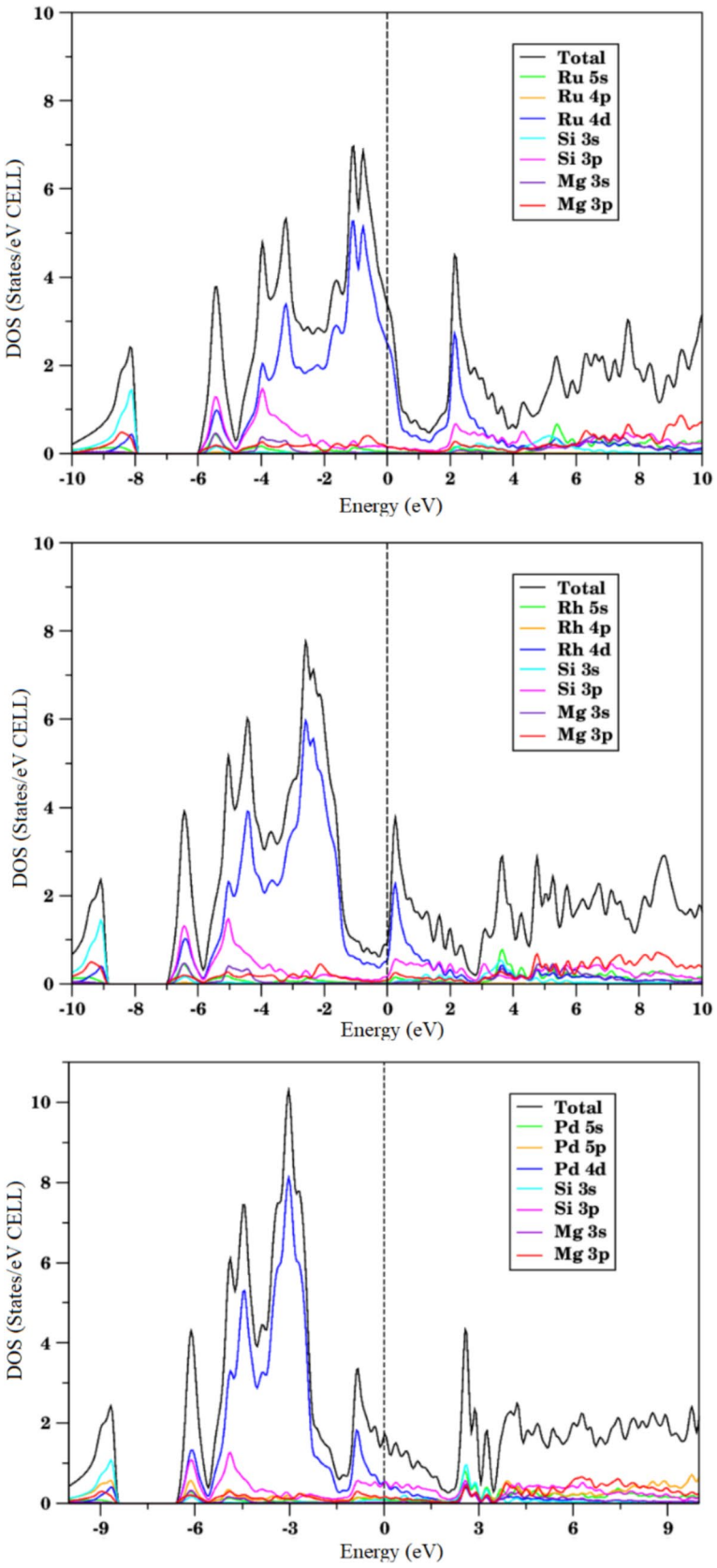

Fig. 3 The computed total and partial DOS plots of full Heusler alloys X_2MgSi (X = Ru, Rh, Pd)

Table 2 The obtained values for the bulk modulus (B, GPa), shear modulus (G, GPa), B/G ratio, Cauchy pressure (CP), Young's modulus (E, GPa), Poisson's ratio (σ), elastic anisotropy factor (A), The specific heat capacity C_V at 300 K (room temperature), Vickers hardness (GPa), Melting temperature (K), the Debye temperature (θ_D) and average velocities of sound (V_{avg}) of the X_2MgSi (X = Ru, Rh, Pd)

Alloy	*B*	*G*	*B/G*	*CP (C_{12}-C_{44})*	*E*	*σ*	*A*	*C_V at 300 K (J/Kmol)*	*H_v*	*T_m*	*θ_D (K)*	*V_{avg} (m/s)*
Ru_2MgSi	198.399	83.946	2.363	58.259	220.710	0.31	0.889	85.182	19.375	2435.000	457.606	3651.620
Rh_2MgSi	183.966	62.304	2.837	78.347	167.948	0.34	1.460	91.028	13.786	2031.475	392.741	3139.741
Pd_2MgSi	135.361	20.163	6.713	95.887	57.550	0.42	3.475	96.201	3.917	1428.081	223.244	1838.634

the elastic constants were obtained from the Voigt-Reuss-Hill approximation [29, 30]:

$$B = \frac{C_{11} + 2C_{12}}{3} \tag{2}$$

$$G_V = \frac{C_{11} - C_{12} + 3C_{44}}{5} \tag{3}$$

$$G_R = \frac{5(C_{11} - C_{12})C_{44}}{4C_{44} + 3(C_{11} - C_{12})} \tag{4}$$

$$G = \frac{G_V + G_R}{2} \tag{5}$$

$$E = \frac{9BG}{3B + G} \tag{6}$$

$$\upsilon = \frac{3B - 2G}{2(3B + G)} \tag{7}$$

$$A = \frac{2C_{44}}{C_{11} - C_{12}} \tag{8}$$

$$C'' = C_{12} - C_{44} \tag{9}$$

To estimate the Vickers hardness (H_v) of the investigated alloys, we employed the empirical model proposed by Chen [31], which correlates hardness with the bulk modulus (B) and shear modulus (G) through the relationship $H_v = 2(k^2G)^{0.585} - 3$, where k = G/B. This model was selected due to its widespread validation for polycrystalline materials, particularly for intermetallic compounds and Heusler alloys, where it provides reliable hardness predictions based solely on first-principles elastic moduli without requiring empirical fitting parameters. Hardness (H_v) represents a crucial mechanical quality that reflects a material's capability to withstand localized deformation [32, 33]. This characteristic is also influenced by structural factors such as defects, grain dimensions, and grain boundaries. The estimated Vickers hardness values are 19.375 GPa for Ru_2MgSi, 13.786 GPa for Rh_2MgSi, and 3.917 GPa for Pd_2MgSi (Table 2). Among these alloys, Ru_2MgSi demonstrates the greatest resistance, whereas Pd_2MgSi shows relatively lower opposition to localized deformation. Ru_2MgSi (19.375 GPa) falls into the moderately hard category, comparable to many transition-metal intermetallics; Rh_2MgSi (13.786 GPa) is classified as medium-hard; and Pd_2MgSi (3.917 GPa) is categorized as soft, exhibiting significantly lower resistance to localized deformation. This classification reflects the trend in their shear moduli and indicates that Ru_2MgSi may be more suitable for applications requiring wear resistance, while Pd_2MgSi could be more amenable to machining and shaping processes.

The melting temperature (T_m) of the X_2MgSi alloys was estimated using the empirical relationship proposed by Fine et al. [26] for cubic materials, which correlates T_m with the elastic constant C_{11}:

$$T_m = 553 + 5.91 \times C_{11} \tag{10}$$

where C_{11} is expressed in GPa and T_m is obtained in Kelvin. This formula was originally derived from pure metals and has been successfully extended to intermetallic compounds and Heusler alloys as a reliable approximation. The calculated T_m values for Ru_2MgSi, Rh_2MgSi, and Pd_2MgSi are listed in Table 2. The decreasing trend in T_m from Ru to Pd correlates with the decreasing C_{11} elastic constant, reflecting the weakening of interatomic bonding strength across the series.

There are no available reference data with which the estimated values can be directly compared. The Cauchy pressure, Poisson's ratio (σ), and Pugh ratio (B/G) are commonly employed to assess the ductile or brittle nature of an alloy [34, 35]. Positive values for Cauchy pressure indicate ductile behavior, whereas negative values suggest brittleness. As shown clearly in Table 2, the predicted CP values for the alloys investigated are all positive, indicating that these alloys are ductile. The positive Cauchy pressures (C_{12}–C_{44}) observed for all three compounds—58.259 GPa (Ru_2MgSi), 78.347 GPa (Rh_2MgSi), and 95.887 GPa (Pd_2MgSi) — indicate the dominance of metallic bonding over directional covalent bonding. The increasing trend in the Cauchy pressure from Ru to Pd reflects the progressive reduction in the

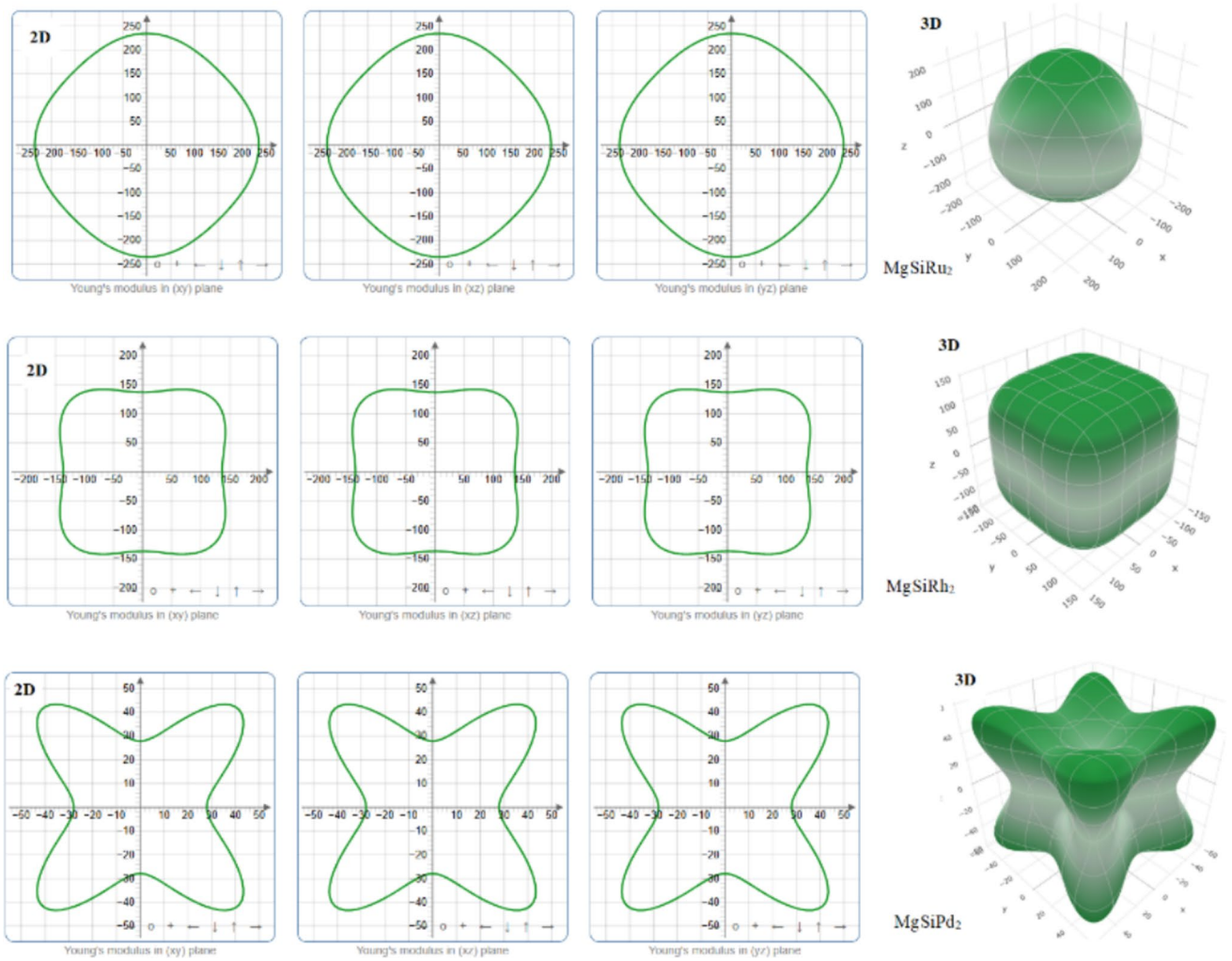

Fig. 4 2D and 3D directional dependences of Young's modulus of full Heusler alloys X_2MgSi (X = Ru, Rh, Pd)

directional bonding character, consistent with the decreasing d-orbital localization across the series.

Poisson's ratio is a key parameter for understanding the deformation behavior of materials under applied stress. The threshold value of Poisson's ratio is generally taken as 0.26. When Poisson's ratio (σ) exceeds this threshold, the material is more likely to exhibit ductile behavior; conversely, values below 0.26 suggest a greater tendency toward brittleness. For the investigations Ru_2MgSi, Rh_2MgSi, and Pd_2MgSi alloys, the calculated Poisson's ratio values are found to be 0.31, 0.34, and 0.42, respectively as evidenced in Table 2. These values further confirm the ductile nature of the alloys studied here. Thus, these values provide additional evidence supporting the ductile nature of the alloys examined. The unusually high σ value of 0.42 for Pd_2MgSi approaches the theoretical upper limit for isotropic solids (0.5), indicating near-incompressible volume retention during elastic deformation and a high degree of metallic bonding.

One of the most effective methods for distinguishing between brittle and ductile behavior in solid materials is the use of the B/G ratio as a criterion. According to the empirical Pugh's criterion, a material is considered ductile if its B/G ratio exceeds 1.75; otherwise, the material is classified as brittle. For this study, the B/G ratios for $MgSiRu_2$, $MgSiRh_2$, and $MgSiPd_2$ were calculated to be 2.363, 2.837, and 6.713, respectively, indicating the ductile nature of the investigated alloys. As a result, the alloys investigated are found to exhibit ductility, and anisotropic behavior. The elastic characteristics obtained highlight the potential suitability of these alloys for use in a range of advanced electronic applications.

The anisotropy observed in the physical properties of crystals stems from variations in bonding along different crystallographic directions. Elastic anisotropy significantly influences numerous crystal characteristics, including phase transformations, internal friction, distinctive phonon modes,

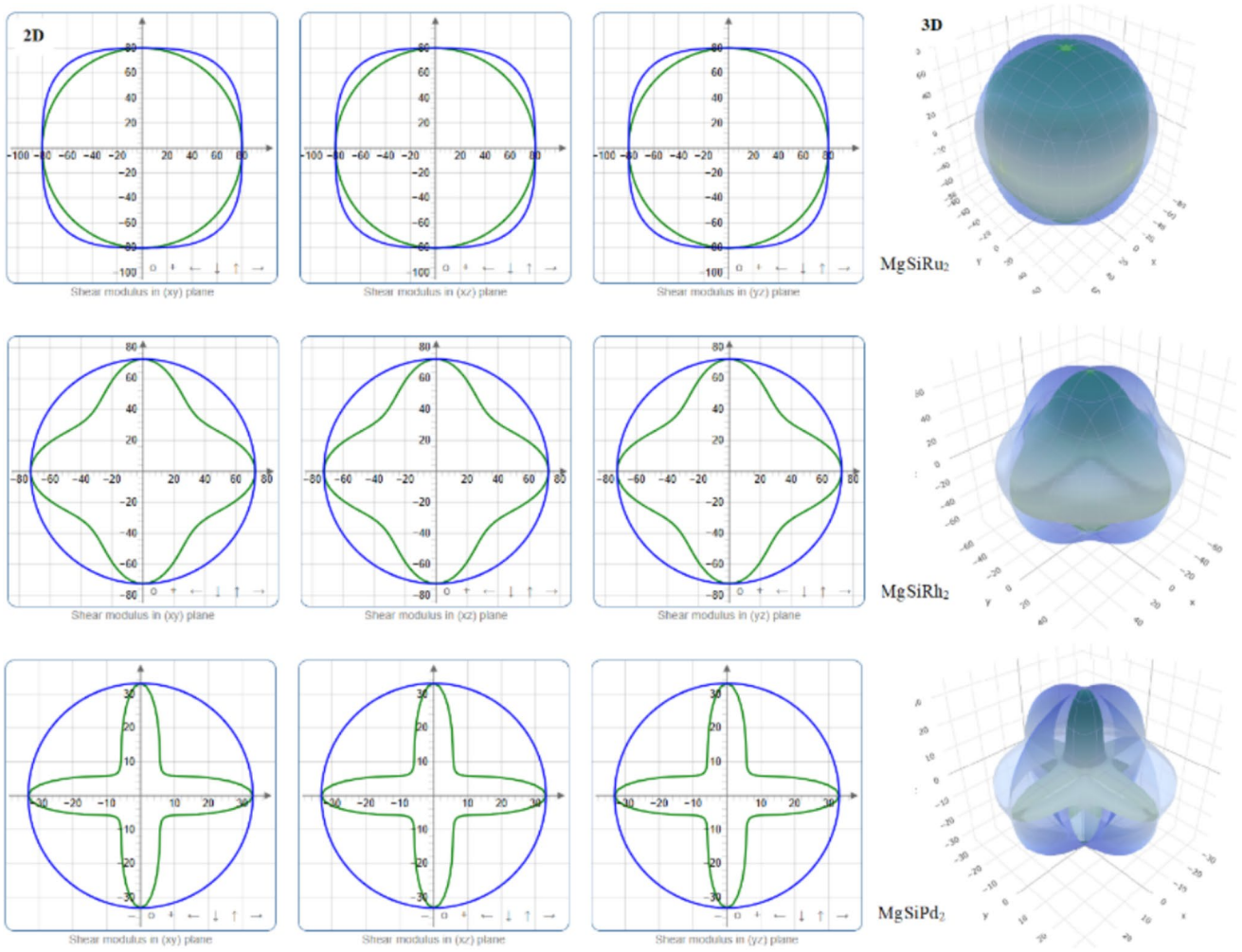

Fig. 5 2D and 3D directional dependences of shear modulus of full Heusler alloys X_2MgSi (X = Ru, Rh, Pd)

and crack propagation behavior. Accordingly, evaluating the degree of elastic anisotropy is crucial for anticipating its effects on related physical phenomena. Both three-dimensional (3D) and two-dimensional (2D) representations provide effective tools to visualize this directional dependence. In an isotropic elastic modulus scenario, the 3D plot forms a perfect closed sphere, while the 2D projection appears as a circle, reflecting uniform mechanical response in all directions. Deviations from these ideal shapes in either the 3D or 2D visuals reveal the level of anisotropy exhibited by the elastic modulus under consideration. The calculated anisotropy factors for X_2MgSi (X = Ru, Rh, and Pd) alloys are listed in Table 2, and their deviation from unity indicates anisotropic behavior in these alloys. The elastic anisotropy factors (A) deviate significantly from unity, with values of 0.889 (Ru_2MgSi), 1.460 (Rh_2MgSi), and 3.475 (Pd_2MgSi). Pd_2MgSi exhibits the strongest anisotropy, meaning that its mechanical response—such as crack propagation and elastic deformation— varies substantially with crystallographic orientation. This behavior arises from the anisotropic charge distribution around Pd atoms, as reflected in the partial DOS showing strong directional hybridization between the Pd 5 d and Si 2p orbitals.

A comprehensive analysis of the directional dependence of elastic anisotropy for the investigated materials was carried out using two-dimensional (2D) and three-dimensional (3D) plots of Young's modulus, shear modulus, and Poisson's ratio, generated via the ELATE software [36], and the results are illustrated in Figs. 4, 5 and 6. The directional variations in Young's modulus, shear modulus, and Poisson's ratio confirm that all three materials exhibit anisotropic behavior in terms of these elastic properties.

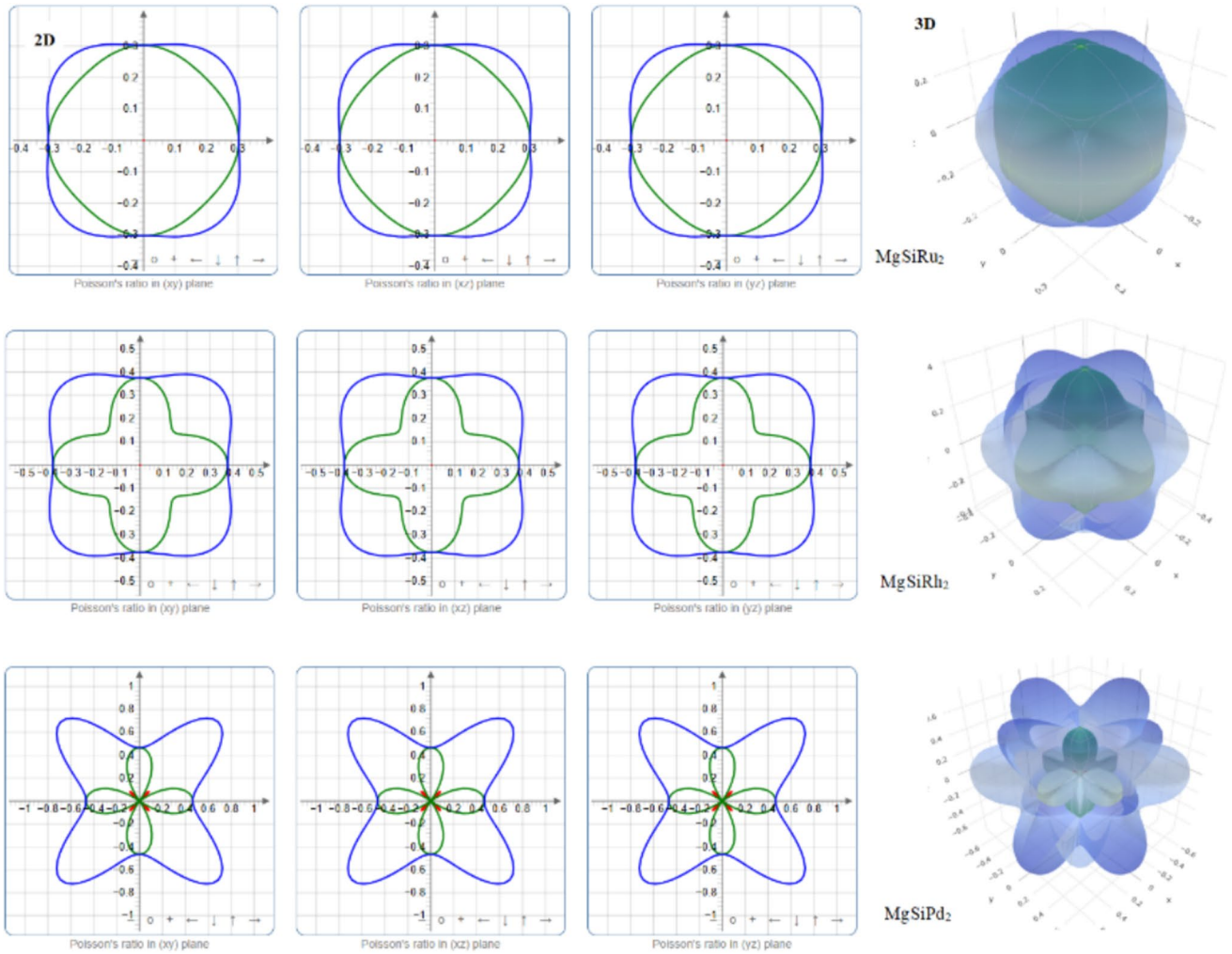

Fig. 6 2D and 3D directional dependences of Poisson's ratio of full Heusler alloys X_2MgSi (X = Ru, Rh, Pd)

Phonon properties

To acquire detailed information on the dynamic stability of X_2MgSi (X = Ru, Rh, and Pd) alloys in the full Heusler phase, we calculated the full phonon dispersion spectra, total and partial density of states (DOS), along high symmetry directions in the Brillouin zone using density functional perturbation theory (DFPT). Figure 7 presents the calculated phonon dispersion curves and phonon state density curves for the three materials. The predicted full phonon dispersion curves and phonon density of states (DOS) profiles for all three materials exhibit a high degree of similarity. Since X_2MgSi alloys contain four atoms per unit cell, they give rise to a total of 12 phonon modes, comprising three acoustic branches and nine optical branches.

The acoustic phonon modes are in the low-frequency region of the dispersion curves, whereas the optical modes are distributed over the higher frequency range [37]. Accordingly, the acoustic modes consist of three branches: one longitudinal acoustic (LA) mode and two transverse acoustic (TA) modes. As illustrated in Fig. 6, the absence of imaginary frequencies in the phonon dispersion curves confirms the dynamic stability of the X_2MgSi alloys. All three analyzed alloys display phonon band gaps in their full dispersion spectra, which can be attributed to the mass differences among the constituent atoms. The presence of a distinct phonon band gap in all three compounds stems from the significant mass difference between the heavier X-region atoms (Ru, Rh, Pd) and the lighter Mg and Si atoms. In such systems, acoustic branches dominated by the vibrations of heavier atoms are well separated from optical branches containing the vibrations of lighter atoms. This gap is particularly pronounced in Pd_2MgSi due to the maximum mass difference between Pd and Si.

A deeper interpretation of the phonon dispersion spectra is emphasized by the total and partial phonon density of states presented in Fig. 8. Low-frequency modes (< 3 THz) are exclusively contributed by Ru/Rh/Pd atoms,

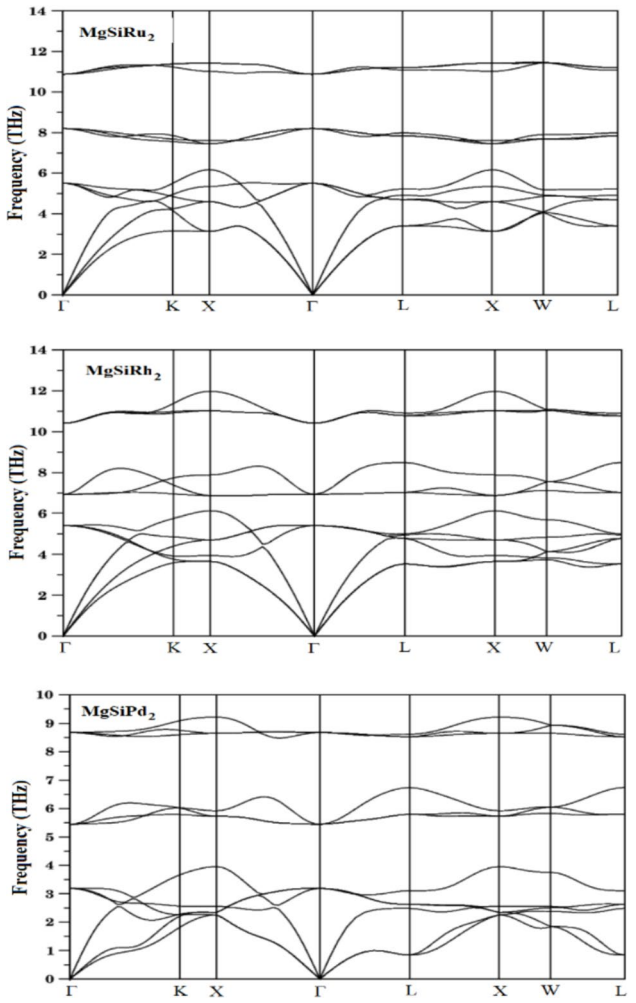

Fig. 7 The evaluated full phonon spectra of full Heusler alloys X_2MgSi (X = Ru, Rh, Pd)

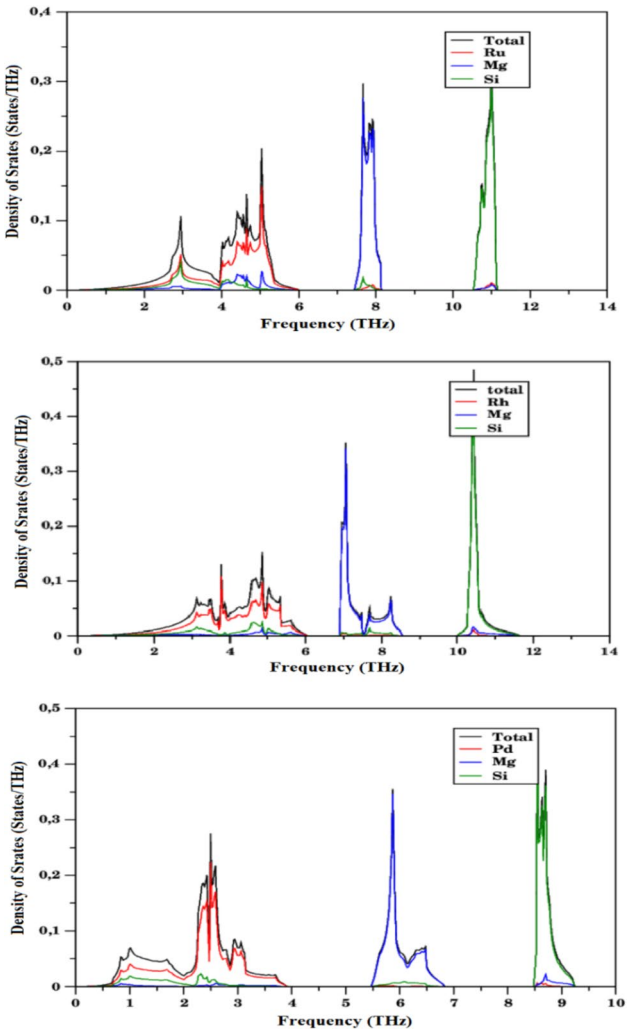

Fig. 8 The evaluated total and partial phonon DOS of full Heusler alloys X_2MgSi (X = Ru, Rh, Pd)

intermediate-frequency modes (3–6 THz) originate from Mg vibrations, and high-frequency modes (> 6 THz) are dominated by Si vibrations. This hierarchical distribution confirms that vibrational dynamics are primarily governed by atomic mass differences rather than bonding strength variations. In general, low-frequency acoustic modes are primarily associated with the vibrations of heavier atoms, whereas high-frequency optical modes originate from the vibrations of lighter atoms. From the partial density of states curves, the top optical modes in all three alloys are derived from the vibrations of Si atoms, the middle optical modes come from the vibrations of Mg atoms, and the lower frequency region consisting of the acoustic and lowest optical modes is derived entirely from the Ru (Rh and Pd) atoms.

The absence of virtual frequencies throughout the Brillouin region proves that all three X_2MgSi compounds have a dynamically stable $L2_1$ structure. This stability criterion is crucial for experimental synthesis, as materials with virtual phonon modes are likely to experience structural instabilities or phase transformations at finite temperatures.

Thermodynamic properties

The Debye model quasiharmonic method was implemented in the Gibbs code to figure out the thermodynamic properties of the X_2MgSi alloys [38]. The internal energy, free energy, entropy, and specific heat capacity at constant volume (C_v) were plotted as functions of temperature, as illustrated in Fig. 9. The Debye temperature (θ_D), calculated from the mean speed of sound, follows the order Ru_2MgSi (457.6 K) > Rh_2MgSi (392.7 K) > Pd_2MgSi (223.2 K). This trend is directly related to elastic stiffness: a higher θ_D implies stronger interatomic bonding and higher thermal conductivity. It is predicted that Ru_2MgSi with the highest

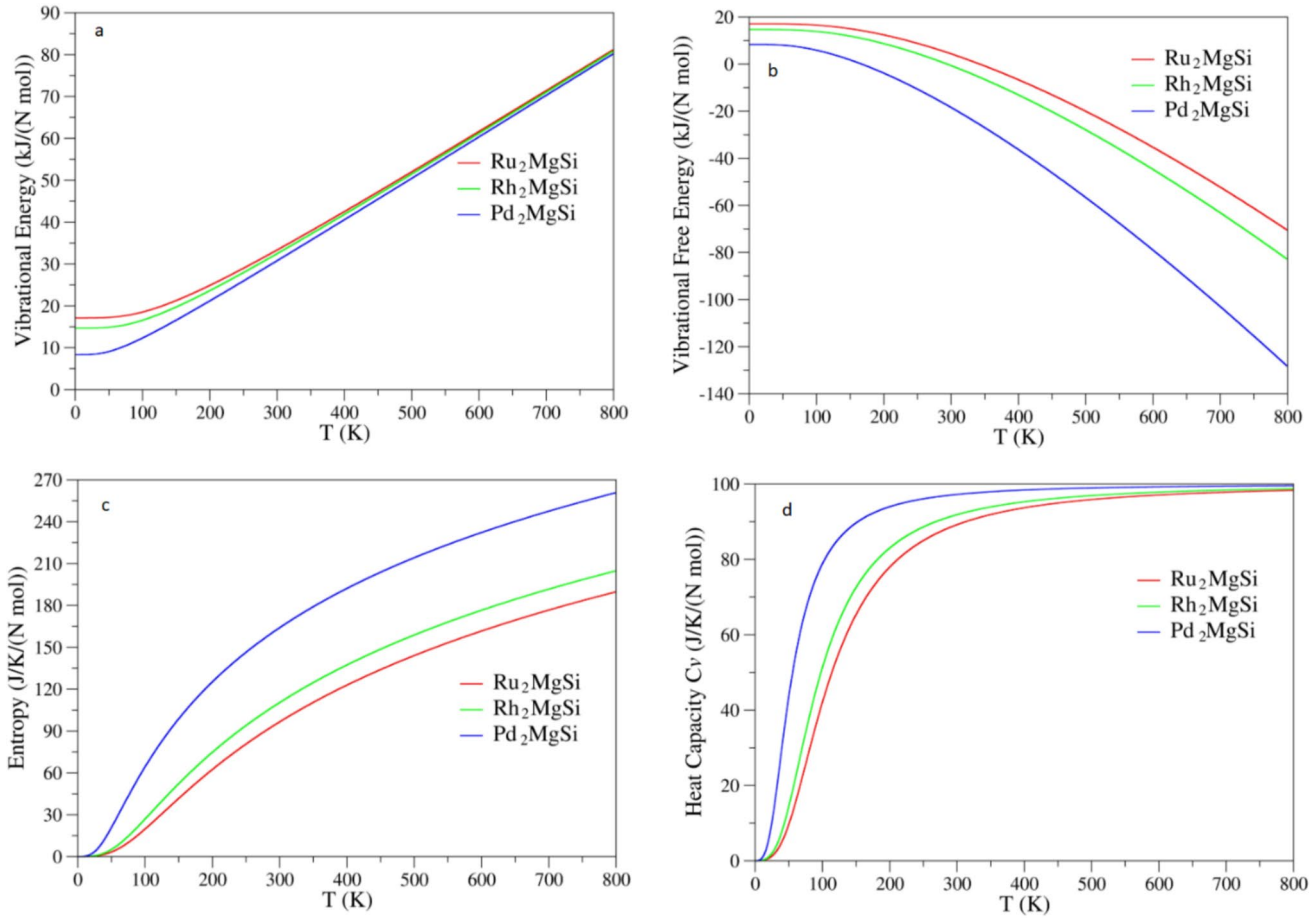

Fig. 9 Evolution of (**a**) vibrational energy, (**b**) vibrational free energy, (**c**) entropy, and (**d**) heat capacity at constant volume as a function of temperature for X_2MgSi alloys

θ_D will have superior thermal conductivity properties and will therefore be potentially suitable for heat dissipation applications.

At temperatures below 100 K, the heat capacity (C_v) follows the Debye T^3 law, characteristic of acoustic phonon dominance. As the temperature increases, C_v approaches the Dulong–Petit limit (~ 99.8 J/K·mol for ternary compounds), indicating full excitation of all vibrational modes. The convergence behavior across the three compounds suggests similar phonon dispersion characteristics, consistent with their structural similarity. Specifically, the value of C_v is observed to drop progressively with the application of higher pressure. This establishes a direct, inverse correlation between these two parameters within this thermal regime. At room temperature (300 K), key thermodynamic quantities such as specific heat capacity (C_v), Debye temperature, and average sound velocities for the studied alloys were also determined, with the results summarized in Table 2. According to C_v and Debye temperature values, the stiffness of the materials is going from higher to lower as $Ru_2MgSi > Rh_2MgSi > Pd_2MgSi$. Ru_2MgSi has the highest thermal conductivity among others considering its Debye temperature and sound velocity.

The temperature-dependent increase in vibrational entropy is fastest for Pd_2MgSi, reflecting smoother phonon modes and a lower Debye temperature (Table 2). This behavior implies that Pd_2MgSi undergoes more significant thermodynamic stabilization with increasing temperature compared to Ru_2MgSi and Rh_2MgSi.

The mean sound velocity (v_{avg}) decreases from 3651.6 m/s (Ru_2MgSi) to 1838.6 m/s (Pd_2MgSi), consistent with the decreasing shear modulus (Table 2). This correlation confirms the reliability of the calculated elastic constants and provides a basis for predicting thermal conductivity.

Among the three X_2MgSi compounds, Pd_2MgSi exhibits notably lower Vickers hardness (3.917 GPa), melting temperature (1428 K), and Debye temperature (223.2 K) compared to Ru_2MgSi and Rh_2MgSi. These trends are

intrinsically linked to the electronic structure and bonding characteristics of the constituent elements.

The sharp decrease in hardness and elastic modulus from Ru to Pd can be attributed to the progressive filling of the d-orbital. Ru ($4d^7$) and Rh ($4d^8$) have partially filled d-shells, enabling strong directional covalent bonding through d–p hybridization with Si. In contrast, Pd ($4d^{10}$) possesses a fully occupied d-band, which significantly reduces the contribution of covalent bonding and enhances the metallic character. This is reflected in the lower shear modulus (20.163 GPa for Pd_2MgSi versus 83.946 GPa for Ru_2MgSi) and the higher Pugh ratio (B/G = 6.713), indicating predominantly metallic bonding with reduced directional strength.

The melting temperature, estimated from the elastic constant C_{11} via the Fine relation [25], follows the same decreasing trend (C_{11}: 318.463 GPa for $Ru_2MgSi \rightarrow$ 148.068 GPa for Pd_2MgSi). This correlation confirms that the thermal stability of these compounds is directly governed by the strength of interatomic bonding, with Pd_2MgSi exhibiting the weakest bond strength.

The Debye temperature (θ_D), which is a measure of lattice stiffness and phonon velocities, decreases from 457.6 K (Ru_2MgSi) to 223.2 K (Pd_2MgSi). This reduction is reliable with the decreasing average sound velocity (v_{avg}: 3651.6 m/s → 1838.6 m/s) and reflects the softening of the lattice upon substitution of Ru by heavier and more electron-rich Pd. A lower θ_D implies a reduced thermal conductivity and a greater propensity for phonon scattering, which may be advantageous for thermoelectric applications but disadvantageous for thermal management [39].

From an application perspective, the combination of low hardness and high ductility in Pd_2MgSi makes it suitable for applications requiring formability, such as thin-film interconnects or composite matrix materials. However, its lower thermal stability and mechanical strength may limit its use in high-temperature structural components, where Ru_2MgSi would be preferred.

Conclusions

In this study, we systematically investigated the structural, elastic, electronic, phonon, and thermodynamic properties of X_2MgSi (X = Ru, Rh, Pd) full-Heusler alloys using first-principles calculations. The electronic, elastic, structural, phonon, and thermodynamic characteristics of X_2MgSi (X = Ru, Rh, and Pd) full-Heusler alloys were explored through density functional theory (DFT) computations within the framework of the GGA-PBE approximation [40, 41]. Our results confirm that all three compounds are structurally, mechanically, and dynamically stable, exhibiting metallic characteristics and ductile behavior. The enthalpies of formation, elastic constants, and phonon dispersions collectively establish a comprehensive property database for these previously unexplored materials. The obtained phonon dispersion relations and projected density of states confirm that the alloys are dynamically stable in the $L2_1$ structure. In addition, the thermodynamic characteristics of the X_2MgSi (X = Ru, Rh, and Pd) alloys were systematically analyzed within the framework of the Debye quasiharmonic approximation (QHA) [5]. The computed formation energies for all the compounds were found to be negative, suggesting favorable chemical stability and a high likelihood of experimental synthesizability.

Prior to this study, experimental data were entirely absent, and theoretical reports were limited to isolated structural parameters. By systematically establishing mechanical stability, electronic structure, lattice dynamics, and temperature-dependent thermodynamic behavior, our findings provide a robust theoretical foundation that can guide future experimental synthesis efforts and serve as a benchmark for computational screening of similar Mg-based alloys. The lightweight nature of Mg combined with its favorable mechanical properties suggest its potential utility in structural components for the aerospace and automotive industries where weight reduction is critical.

Furthermore, the metallic character and thermal transport properties (indicated by Debye temperatures) make these compounds worth exploring for thermoelectric applications, particularly in intermediate-temperature ranges. Among these three materials, Ru_2MgSi stands out for its superior mechanical strength and thermal conductivity, while Pd_2MgSi, with its softer nature and higher ductility, may be more suitable for applications requiring formability or as a component in composite materials.

Author Contribution G.D.Y. and Y.G.Y. prepared Figs. 1–9. N.A. wrote the methodology and made the calculations. M.Ç. wrote the introduction, findings, and conclusion. All authors reviewed the manuscript.

Funding No funding was received for conducting this study.

Data Availability No datasets were generated or analysed during the current study.

Declarations

Competing interests The authors declare no competing interests.

References

1. Heusler F (1903) Verh Dtsch Phys Ges 5:219
2. Hayashi K, Li H, Eguchi M, Nagashima Y, Miyazaki Y (2020) Magnetic full-Heusler compounds for thermoelectric applications. Magn Mater Magn Levit 65.

3. Al-Douri Y, Ameri M (2025) Physical studies of spintronics-based Heusler alloys. Crit Rev Solid State Mater Sci 50(2):189–238. https://doi.org/10.1080/10408436.2024.2407463
4. Özdoğan K, Galanakis I (2024) Interplay between structural, electronic, and magnetic properties in the d 0-d semi-Heusler compounds; the case of the K-based compounds. Solids 5(4):533–543. https://doi.org/10.3390/solids5040036
5. Özer T, Çanlı M, Arıkan N, Öztürk Aİ (2025) First-principles calculations to investigate the structural, elastic and thermodynamic properties of full-Heusler $MgXY_2$ (X= Zn, Cd, Y= Ag, Au, Cu) compounds. J Mag Alloys 13(5):2295–2306. https://doi.org/10.1016/j.jma.2025.03.012
6. Zhang Z, Gurtaran M, Dong H (2024) Low-cost magnesium-based thermoelectric materials: progress, challenges, and enhancements. ACS Appl Energy Mater 7(14):5629–5646
7. Xie J, Zhang T, Jiang J, Xue W, Wang W, Ni J, Zhang X, Liu X (2025) Advances in magnesium-based implants for biomedical applications: a comprehensive review and future perspectives. J Magnes Alloys 13(7):2978–3003. https://doi.org/10.1016/j.jma.2025.05.009
8. Winiarski MJ, Kuderowicz G, Górnicka K, Litzbarski LS, Stolecka K, Wiendlocha B, Cava RJ, Klimczuk T (2021) MgPd2Sb: a Mg-based Heusler-type superconductor. Phys Rev B 103(21):214501. https://doi.org/10.1103/PhysRevB.103.214501
9. Batalović K, Radaković J, Kuzmanović B, Ilić MM, Mamula BP (2023) Machine learning-based high-throughput screening of Mg-containing alloys for hydrogen storage and energy conversion applications. J Energy Storage 68:107720. https://doi.org/10.1016/j.est.2023.107720
10. Shen J, Griesemer SD, Gopakumar A, Baldassarri B, Saal JE, Aykol M, Hegde VI, Wolverton C (2022) Reflections on one million compounds in the open quantum materials database (OQMD). J Phys Mater 5(3):031001. https://doi.org/10.1088/2515-7639/ac7ba9
11. Baskaran P, Muthiah B, Uthirapathy V (2025) A systematic review on biomaterials and their recent progress in biomedical applications: bone tissue engineering. Rev Inorg Chem 45(4):747–781. https://doi.org/10.1515/revic-2024-0062
12. Lin Y, Yu W, Wang G, Li Z, Jiang Y, Feng J, Chong X (2024) Exploring the effect of alloying elements on the thermoelasticity and strength of bcc Fe-based alloys by first-principles phonon calculations. J Mater Res Technol 30:954–965. https://doi.org/10.1016/j.jmrt.2024.03.101
13. Kohn W (1996) Density functional and density matrix method scaling linearly with the number of atoms. Phys Rev Lett 76:3168. https://doi.org/10.1103/PhysRevLett.76.3168
14. Roondhe B, Giannozzi P (2025) Dual-metal porphyrin–graphene hybrids as oxygen catalysts: comparative DFT insights into O_2 adsorption and activation. J Chem Phys 163(22):224703. https://doi.org/10.1063/5.0303648
15. Peng H, Perdew JP (2017) Rehabilitation of the Perdew-Burke-Ernzerhof generalized gradient approximation for layered materials. Phys Rev B 95(8):081105. https://doi.org/10.1103/PhysRevB.95.081105
16. Kohn W, Sham LJ (1965) Self-consistent equations including exchange and correlation effects. Phys Rev B 140(4A):A1133. https://doi.org/10.1103/PhysRev.140.A1133
17. Monkhorst HJ, Pack JD (1976) Special points for Brillouin-zone integrations. Phys Rev B 13(12):5188. https://doi.org/10.1103/PhysRevB.13.5188
18. Giannozzi P, Baseggio O, Bonfà P, Brunato D, Car R, Carnimeo I, Cavazzoni C, de Gironcoli S, Delugas P, Ruffino FF, Ferretti A, Marzari N, Timrov I, Urru A, Baroni S (2020) Quantum ESPRESSO toward the exascale. J Chem Phys. https://doi.org/10.1063/5.0005082
19. Giannozzi P, Andreussi O, Brumme T, Bunau O, Nardelli MB, Calandra M, Car R, Cavazzoni C, Ceresoli D, Cococcioni M (2017) Advanced capabilities for materials modelling with quantum ESPRESSO. J Phys Condens Matter 29(46):465901. https://doi.org/10.1088/1361-648X/aa8f79
20. Nielsen OH, Martin RM (1983) First-principles calculation of stress. Phys Rev Lett 50:697. https://doi.org/10.1103/PhysRevLett.50.697
21. Fioccola S, Giacomazzi L, Ceresoli D, Richard N, Hemeryck A, Martin-Samos L (2025) An open-source package for the Quantum ESPRESSO distribution to compute non-perturbatively orbital magnetization from first principles, including NMR chemical shifts and EPR parameters. Comput Phys Commun 109891. https://doi.org/10.1016/j.cpc.2025.109891
22. Pan Y, Chen S (2020) Exploring the novel structure, transportable capacity and thermodynamic properties of TiH2 hydrogen storage material. Int J Energy Res 44(6):4997–5007. https://doi.org/10.1002/er.5260
23. Horton MK, Huck P, Yang RX et al (2025) Accelerated data-driven materials science with the materials project. Nat Mater 24:1522–1532. https://doi.org/10.1038/s41563-025-02272-0
24. Arıkan N, Örnek O, İyigör A, Çanlı M (2024) Investigation on the structural, elastic, electronic, thermodynamic, and vibrational properties of the full heusler Sc2XAl (X= Cd and Zn): an ab initio study. Physica B 695:416492. https://doi.org/10.1016/j.physb.2024.416492
25. Xu N, Chen Y, Chen S, Li S, Zhang W (2024) First-principles investigation for the hydrogen storage properties of XTiH3 (X=K, Rb, Cs) perovskite type hydrides. Int J Hydrogen Energy 50:114–122. https://doi.org/10.1016/j.ijhydene.2023.06.254
26. Fine ME, Brown LD, Marcus HL (1984) Elastic constants versus melting temperature in metals. Scr Metall 18(9):951–956. https://doi.org/10.1016/0036-9748(84)90267-9
27. Chacko Z, Cance J, Rabiei A (2025) Evaluating elastic modulus and energy absorption efficiency of composite metal foam using computational and experimental approaches. J Mater Sci 60(19):7942–7964. https://doi.org/10.1007/s10853-025-10905-7
28. Born M, Huang K (1996) Dynamical theory of crystal lattices. Oxford university press
29. Wafula JW (2023) Structural, elastic, electronic, optical and thermal properties of YMAu (M= Si or Ge or Sn) half-heusler compounds; a DFT study. Results Mater 19:100413. https://doi.org/10.1016/j.rinma.2023.100413
30. Bhaskar LK, Moharana N, Holz H, Ramachandramoorthy R, Kumar KH, Kumar R (2025) Probing elastic isotropy in entropy stabilized transition metal oxides: experimental estimation of single crystal elastic constants from polycrystalline materials. Acta Mater 288:120871
31. Dovale-Farelo V, Tavadze P, Lang L, Bautista-Hernandez A, Romero AH (2022) Vickers hardness prediction from machine learning methods. Sci Rep 12(1):22475
32. Pintaude G (2023) Hardness as an indicator of material strength: a critical review. Crit Rev Solid State Mater Sci 48(5):623–641. https://doi.org/10.1080/10408436.2022.2085659
33. Wafula JW, Manyali GS (2025) Structural, mechanical, and thermal properties of Mo2MB2 (M= Ti, Zr and Hf) super-alloys from first-principles approach. Next Mater 8:100715
34. Niu J, Miao B, Guo J, Ding Z, He Y, Chi Z, Wang F, Ma X (2023) Leveraging deep neural networks for estimating Vickers' hardness from nanoindentation hardness. Materials 17(1):148. https://doi.org/10.3390/ma17010148
35. Senkov ON, Miracle DB (2021) Generalization of intrinsic ductile-to-brittle criteria by Pugh and Pettifor for materials with a cubic crystal structure. Sci Rep 11(1):4531
36. Feng R, Kim G, Yu D, Chen Y, Chen W, Liaw PK, An K (2022) Elastic behavior of binary and ternary refractory

multi-principal-element alloys. Mater Des 219:110820. https://doi.org/10.1016/j.matdes.2022.110820
37. Ran Z, Zou C, Wei Z, Wang H (2023) VELAS: an open-source toolbox for visualization and analysis of elastic anisotropy. Comput Phys Commun 283:108540. https://doi.org/10.1016/j.cpc.2022.108540
38. Assouar MB, Oudich M (2011) Dispersion curves of surface acoustic waves in a two-dimensional phononic crystal. Appl Phys Lett. https://doi.org/10.1063/1.3626853
39. Wafula JW, Makokha JW, Manyali GS (2022) First-principles calculations to investigate structural, elastic, electronic and thermodynamic properties of NbCoSn and VRhSn Half-Heusler compounds. Results Phys 43:106132. https://doi.org/10.1016/j.rinp.2022.106132
40. Daoud S, Bioud N, Saini PK (2019) Finite temperature thermophysical properties of MgCu intermetallic compound from quasi-harmonic Debye model. J Mag Alloys 7(2):335–344. https://doi.org/10.1016/j.jma.2019.01.006
41. Zoubair AB, Samih A, El Fdil R, Nfissi A, Es-Semyhy M, Salmani E, ... Husain FM (2025) GGA and GGA+ U investigation of half-metallic ferromagnetism in cubic $EuVO_3$ perovskite. J Mol Graphics Modell 109182. https://doi.org/10.1016/j.jmgm.2025.109182